IET Electric Power Applications

Research Article

IET Journals
The Institution of Engineering and Technology

Analysis of magnetic-coupling effect on the performances of 2DoF direct-drive induction motors

ISSN 1751-8660
Received on 18th December 2017
Revised 11th March 2018
Accepted on 27th March 2018
E-First on 9th May 2018
doi: 10.1049/iet-epa.2017.0842
www.ietdl.org

Peixin Wang[1,2], Jikai Si[1] ✉, Lujia Xie[3], Yihua Hu[3], Wei Hua[2]

[1]*School of Electrical Engineering and Automation, Henan Polytechnic University, Jiaozuo, People's Republic of China*
[2]*School of Electrical Engineering, Southeast University, Si-Pai-Lou No. 2, Nanjing, People's Republic of China*
[3]*Department of Electrical Engineering and Electronics, University of Liverpool, Liverpool, UK*
✉ *E-mail: sijikai527@126.com*

Abstract: The coupling between the rotary and linear magnetic fields is a special feature of two-degrees-of-freedom (2DoF) motors. The magnetic-coupling effect on the performances of 2DoF direct-drive induction motors (2DoF-DDIMs) is exposed and investigated based on 3D finite-element analysis and experiments on a prototyped motor. The performances of the 2DoF-DDIM are analysed under the conditions of with and without coupling. Further, the speed coupling coefficient is introduced and calculated to consider the effect of the magnetic-coupling effect on speed. The magnetic-coupling effect of 2DoF-DDIM, which leads to induced voltages and currents under rotary or linear motion and lower speed and higher fluctuations under helical motion, enhances with an increase in the source frequency and rotary speed. This research on the magnetic-coupling effect of 2DoF-DDIM will provide a significant reference for characteristic research and precise control of 2DoF-DDIM.

1 Introduction

Two-degrees-of-freedom (2DoF) motion, which comprises rotary and linear motions simultaneously, i.e. helical motion, is widely used in industrial machinery such as boring machines, grinders, and electric vehicles [1, 2]. In conventional driving machinery, 2DoF motion is realised by a rotary motor installed on a linear motor or special gears installed on a rotary motor, which inevitably increases the weight of the driving system and reduces its efficiency owing to the additional losses caused by the intermediate transmission mechanism. Therefore, 2DoF motors, which are capable of rotary, linear, and helical motions through the use of a single motor, are of great interest owing to their advantages of integrated structures, small mechanical loss, and high reliability etc.

However, due to the special structures and various motion forms of 2DoF motors, the internal magnetic fields due to rotary and linear motions are complicated and coupled each other. Previously, a two-armature rotary-linear induction motor with the armatures axially connected in series has been researched [3, 4]. However, as indicated by the analysis of the motor characteristics through the finite-element method, the linear magnetic field and motion can weaken the rotary torque and efficiency to some extent [5, 6]. In a subsequent establishment of the equivalent circuit model, this weakening effect was considered in the form of additional magneto-motive force and the computational accuracy was relative high, which was verified by the finite-element model. For the rotary-linear permanent magnet actuator with a Halbach magnet array which can realise a high magnetic load, the static magnetic field was investigated [7] and the two-directional d–q transformation was proposed to decouple the inter-relation between the linear and rotary motions [8]. Further, the interval between two successive magnets in the axial direction affects the rotary and linear magnetic flux densities [9]. For the rotary-linear switched reluctance motor [10, 11], linear force was generated by the coupling of multiple rotary magnetic fields, whose coupling intensity changed with the power supply mode of the motor. A decoupling PID control based on the net torque method was proposed to realise integrated separation between the rotary and linear motions [12].

In addition, an integrated 2DoF motor was proposed and analysed by adopting the permeation depth method and the composite multilayer method [13, 14]. The static coupling effect of the 2DoF-DDIM, which indicates that the special induced voltages and currents are generated in the rotary part, was researched [15]. However, the reason and other characteristics of the magnetic-coupling effect have not been studied yet.

In this study, the magnetic-coupling effect of the 2DoF-DDIM is researched detailedly. A 3D finite-element model is developed to determine the inner coupling magnetic fields and output performances caused by magnetic-coupling effect of the 2DoF-DDIM. The induced voltages and currents, the rotary torque (or linear force), speeds and their corresponding fluctuations are calculated. It can be concluded that the stronger the coupling magnetic field is, the more obvious the magnetic-coupling effect will be. Besides, the difference between the rotary and linear parts under magnetic-coupling effect is explained. Testing is also carried out to validate the existence of the magnetic-coupling effect.

2 Structure and principle of 2DoF-DDIM

A 2DoF-DDIM consists of a rotary arc-shaped armature in the rotary part, a linear arc-shaped armature in the linear part, and a cylindrical solid mover coated with a copper layer shared by the two parts. The rotary part stator core is slotted along the axial direction, while the linear part stator core is slotted along the circumferential direction. The rotary and linear part stators have the same inner and outer diameters. The structure of a 2DoF-DDIM is shown in Fig. 1, and the main structural parameters are summarised in Table 1.

Depending on the power supply mode, the 2DoF-DDIM can produce two forms of air-gap magnetic fields and the corresponding electromagnetic torque or force to directly drive the mover to perform rotary, linear, or helical motion.

Based on the 2DoF-DDIM structure shown in Fig. 1 and the working principle, a 3D finite-element model of the 2DoF-DDIM was established in *Magnet*, as shown in Fig. 2*a*. The distribution of the magnetic field under helical motion is shown in Fig. 2*b*.

The solid model of the 2DoF-DDIM is enclosed in an air-box component with a default flux tangential outer boundary in *Magnet*. The default settings are adopted to achieve reasonable accuracy and avoid errors. Then the model will be fully solved by considering the end effect, the skin effect etc.

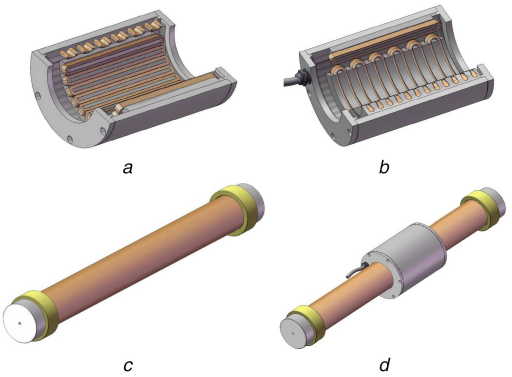

Fig. 1 *Structure of 2DoF-DDIM*
(a) Rotary arc-shaped armature, ***(b)*** Linear arc-shaped armature, ***(c)*** Solid mover, ***(d)*** Assembly of 2DoF-DDIM

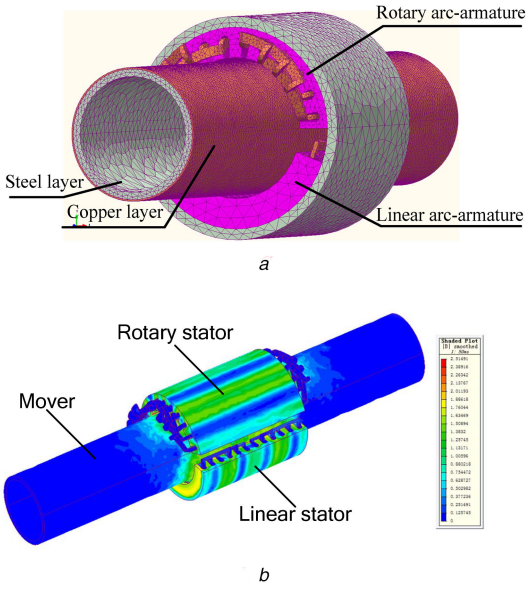

Fig. 2 *3D finite-element model of 2DoF-DDIM*
(a) Solid model, ***(b)*** Distribution of |B|

3 Coupling magnetic field of 2DoF-DDIM

For most 2DoF motors, their rotary magnetic field is coupled with the linear magnetic field. Due to the special structure of a 2DoF-DDIM, when the linear part is energised independently, a linear coupling magnetic field (LCMF), other than the main magnetic field in the linear part, is generated in the rotary part by end effect, as shown in Fig. 3*a*. Similarly, a rotary coupling magnetic field (RCMF) is generated in the linear part when the rotary part is energised, as shown in Fig. 3*b*.

As shown in Fig. 3*a*, the left and right sides of the LCMF are almost symmetrical, but the left side of the RCMF is stronger than the right side. The reason of this phenomenon is that the LMCF is generated by the horizontal end effect of the linear part, while the RCMF is generated by the vertical end effect of the rotary part. Moreover, there are no other factors besides power source that can change the LCMF. However, the rotary speed enhances the magnetic field in the outgoing end of the mover (left side in Fig. 3*b*) and weakens it in the incoming end of the mover (right side in Fig. 3*b*).

Through solving the vector magnetic potential of the rotary coupling magnetic field and coordinate conversion (the process is enclosed in the appendix), the magnetic flux density of the RCMF is derived as

$$B_m = \dot{C}_1 m_1 \mathrm{e}^{m_1(\theta - 2\pi)} - \dot{C}_2 m_2 \mathrm{e}^{-m_2\theta} \tag{1}$$

where

$$\begin{cases} m_1 = \sqrt{\mu_0^2\gamma^2 v^2 + \mathrm{j}\dfrac{\mu_0 w \gamma_2 \Delta}{\delta}} + \mu_0\gamma v \\ m_2 = \sqrt{\mu_0^2\gamma^2 v^2 + \mathrm{j}\dfrac{\mu_0 w \gamma_2 \Delta}{\delta}} - \mu_0\gamma v \end{cases}$$

Here, μ_0, γ, v, w, Δ, γ_2, and δ denote the vacuum permeability, relative conductivity of the mover, the rotary speed, the angular frequency, the conductor plant thickness, the conductivity of the mover, and equivalent electromagnetic air-gap, respectively.

Table 1 Structural parameters of a 2DOF-DDIM

Items of interest	Values/dimension	
	Rotary part	Linear part
rated voltage	220 V	220 V
supply frequency	50 Hz	50 Hz
pole pitch	2	2
stator inner diameter	98 mm	98 mm
stator outer diameter	155 mm	155 mm
stator axial length	156 mm	156 mm
mover outer diameter	96 mm	
mover axial length	600 mm	
copper layer thickness	1 mm	

4 Magnetic-coupling effect of 2DoF-DDIM

From Section 3, it can be concluded that there are the main and coupling magnetic fields generated when the motor is energised. When only one part of the 2DoF-DDIM is powered, the corresponding coupling magnetic field is produced and linked with the other part. Hence, the induced voltages and currents are produced in the windings according to Faraday law of electromagnetic induction. Obviously, this kind of coupling magnetic fields will remain when the 2DoF-DDIM is fully energised. Hence, the coupling magnetic fields will interact with the main ones, which will deteriorate the output performance of the motor.

4.1 Coupling-induced voltage and current

Firstly, the special features, which are caused by magnetic-coupling under rotary or linear motion, are analysed. The induced voltages and currents are produced in the winding without power by the linking with the coupling magnetic field. The value of the induced voltages and currents is determined by the amplitude and frequency of the coupling magnetic field. Hence, the stronger the coupling magnetic field is, the higher the induced voltages will be.

According to the distribution of the coupling magnetic field and the mode of windings, the relation between the three-phase induced voltages and currents of the linear part, which has been verified by reference [12], can be obtained as

$$\begin{cases} U_A \simeq U_B \simeq -U_c \\ I_A \simeq I_B \simeq -\dfrac{1}{2}I_C \end{cases} \tag{2}$$

Furthermore, the relation between the three-phase induced voltages and currents of the rotary part are satisfied with this rule adopting a similar method.

Based on the 3D finite-element model of a 2DoF-DDIM, the linear part is energised with a 220 V, 50 Hz AC source and the rotary part, which is non-powered, is simulated. Then, the induced voltages and currents can be obtained from the rotary part, as shown in Fig. 4.

Similarly, when the rotary part is energised with a 220 V, 50 Hz AC source and the linear part is non-powered, the induced voltages and currents can be obtained from the linear part, as shown in Fig. 5.

Figs. 4 and 5 show that the induced voltages and currents are consistent with (2). Further, their frequencies are equivalent to the supply source frequency. These induced voltages and currents

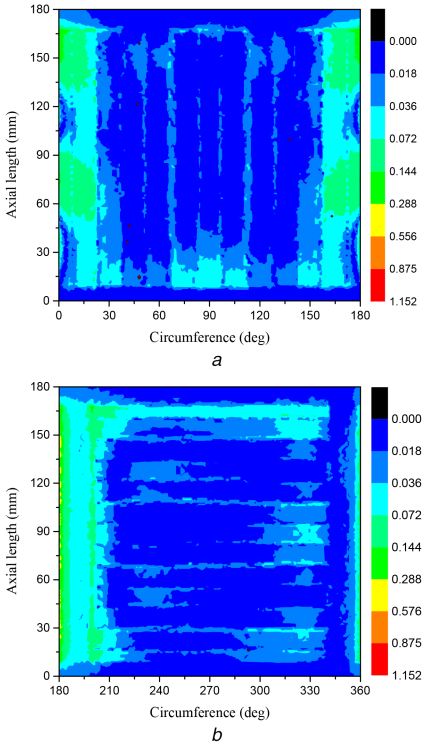

Fig. 3 *Coupling magnetic field of 2DoF-DDIM*
(a) LCMF, ***(b)*** RCMF

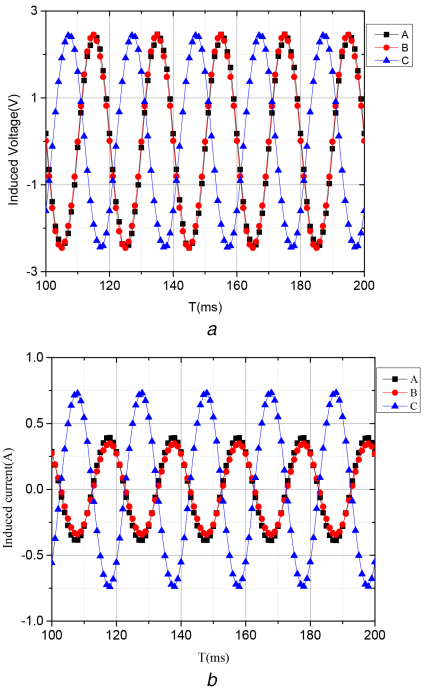

Fig. 4 *Induced voltages and currents of the rotary part*
(a) Induced voltages, ***(b)*** Induced currents

confirm the existence of magnetic-coupling effect of the 2DoF-DDIM.

The induced voltages are closely related to the amplitude and period of the coupling magnetic field. Based on a constant voltage and frequency ratio to maintain the amplitude of the main magnetic field, when the linear part is energised with AC sources of different frequencies (from 10 to 50 Hz), the induced voltages in the rotary part are shown in Fig. 6*a*. Similarly, the induced voltages in the linear part, with AC sources of different frequencies supplied in the rotary part, are shown in Fig. 6*b*.

Fig. 6 shows that the induced voltages of the linear and rotary parts increase with the source frequency. In summary, the

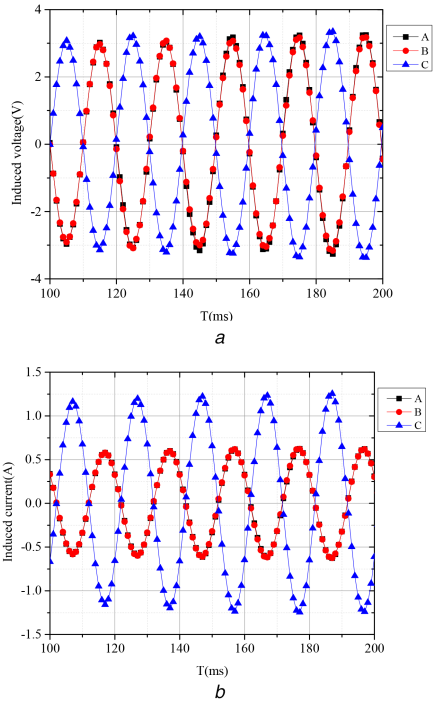

Fig. 5 *Induced voltages and currents of the linear part*
(a) Induced voltages, ***(b)*** Induced currents

magnetic-coupling effect enhances along with the source frequency on a constant voltage and frequency ratio.

From Section 3, the LCMF is generated by the horizontal end effect of the linear part and relates only to the supplied source. However, according to (1), the RCMF changes with the rotary speed, which can be verified by the fact that the RCMF at the outgoing end of the mover is stronger than that at the incoming end, as shown in Fig. 3*b*.

Fig. 7*a* shows the induced voltages in the rotary part, along with different linear slips when the linear part is energised with a 220 V, 50 Hz three-phase AC source independently. Similarly, the induced voltages in the linear part along with different rotary slips are shown in Fig. 7*b*.

From Fig. 7, it can be seen that the induced voltages of the rotary part vary almost linearly with the linear slip, while those of the linear part are nearly halved from the synchronous speed to zero speed. That is, the linear speed has little influence on the magnetic-coupling effect, while the rotary speed enhances the magnetic-coupling effect. In short, the faster the rotary speed is, the stronger the magnetic-coupling effect will be.

According to the above analysis and the simulation results, we can conclude that the magnetic-coupling effect really exists in a 2DoF-DDIM. The induced voltages and currents are generated in the windings by the linkage between the coupling magnetic field and the windings. The magnetic-coupling effect of the 2DoF-DDIM gets stronger with an increase in the source frequency and rotary speed.

4.2 Performances considering MCE

From the above analysis, when the motor is under rotary or linear motion, it can be concluded that special induced voltages and currents will be generated in the unpowered part. As the most special motion form of the motor, the influences caused by magnetic-coupling effect under helical motion are of great significant and should be heeded and researched.

Based on the 3D finite-element model, when the mover is set to zero speed and the linear part is energised using a 220 V, 50 Hz AC source, the forces of the linear part under the conditions of the rotary part non-powered (without coupling) and powered (coupling) are shown in Fig. 8*a*. Similarly, the rotary torques with and without coupling are shown in Fig. 8*b*. The average force (or torque) and its fluctuation are listed in Table 2.

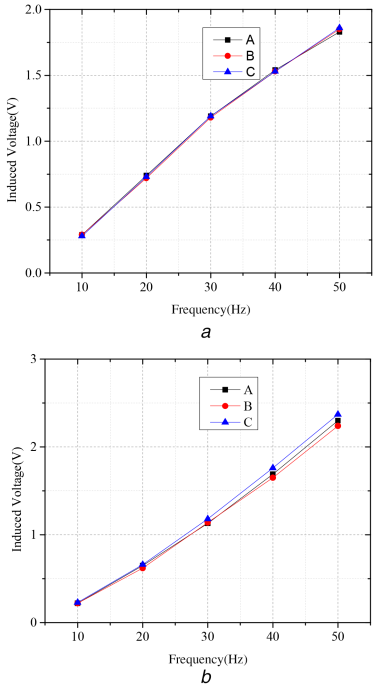

Fig. 6 *Induced voltages along with source frequency*
(a) Linear part, ***(b)*** Rotary part

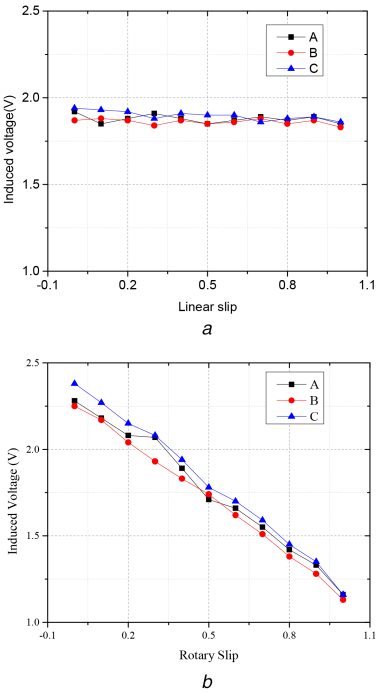

Fig. 7 *Induced voltages along with motor slips*
(a) Linear part, ***(b)*** Rotary part

A comparison of the simulation results under the conditions of with and without coupling from Fig. 8 and Table 2 shows that the average force is reduced by 1 N and the average torque is reduced by 0.3 Nm, while their fluctuations are more than doubled. Overall, the magnetic-coupling effect has little influence on the average force (or average torque) but causes more than two times fluctuation.

Based on the 3D finite-element model, when the mover is set to no load for the linear part and zero speed for the rotary part, and the linear part is energised using a 220 V, 50 Hz AC source, the speeds of the linear part under the conditions of the rotary part non-powered (without coupling) and powered (coupling) are shown in Fig. 9*a*. Similarly, the rotary speeds with and without coupling are shown in Fig. 9*b*. The average speed and their fluctuation are listed in Table 3.

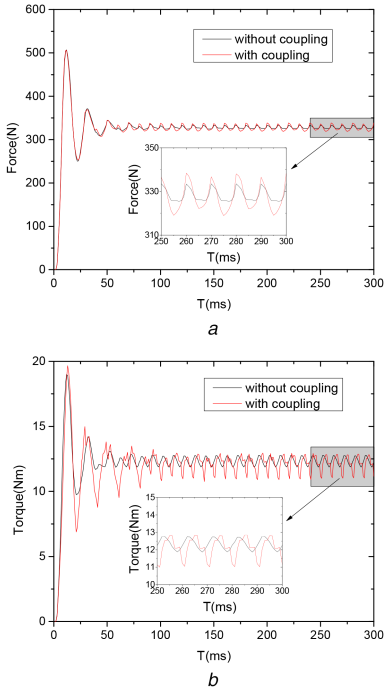

Fig. 8 *Magnetic force curves of 2DoF-DDIM*
(a) Linear force, ***(b)*** Rotary torque

Table 2 Average force and torque of 2DoF-DDIM

Items		Without coupling	With coupling
linear force, N	average	328.3	327.3
	fluctuation	2.903	6.236
rotary torque, Nm	average	12.34	12.09
	fluctuation	0.30	0.61

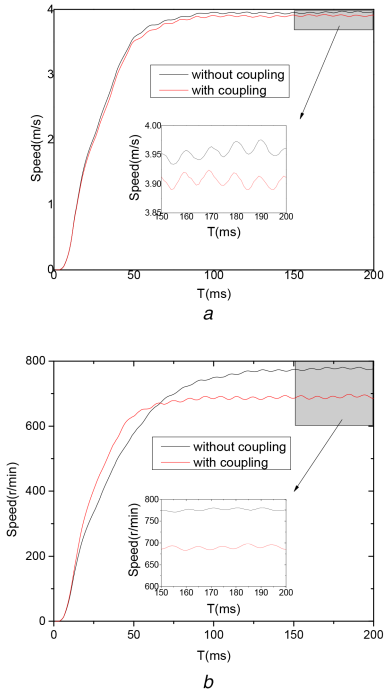

Fig. 9 *Speed of 2DoF-DDIM*
(a) Linear speed, ***(b)*** Rotary speed

According to Fig. 9 and Table 3, due to the magnetic-coupling effect, the linear average speed is reduced by 1.1% and its fluctuation is increased by 6.2%, while the rotary average speed is reduced by 10.8% and its fluctuation is enhanced by 50.9%.

Table 3 Speed of 2DoF-DDIM

Items		Without coupling	With coupling
linear speed, m/s	average	3.949	3.907
	fluctuation	0.0081	0.0086
rotary speed, r/min	average	774.5	690.8
	fluctuation	2.22	3.35

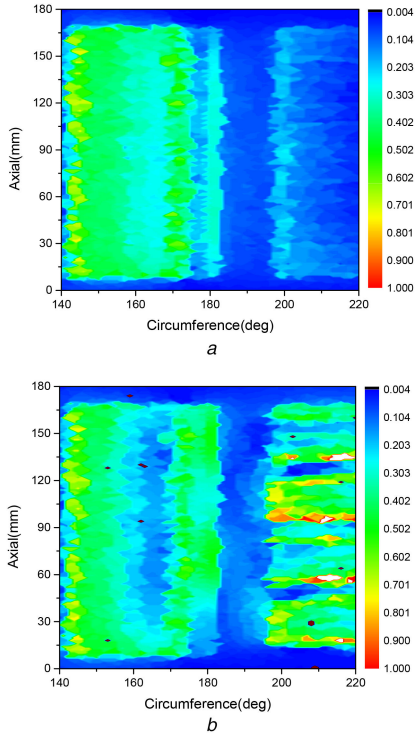

Fig. 10 *End magnetic field of the rotary part*
(a) Without coupling, ***(b)*** With coupling

We find that the changes in speed and its fluctuation in the rotary part are nearly ten times as much as those in the linear part in the presence of a coupling magnetic field. The rotary part of the 2DoF-DDIM is more significantly influenced by the magnetic-coupling effect compared to the linear part. This is because the magnetic-coupling effect not only changes the distribution of the main magnetic field of the rotary part but also reduces the 'equivalent electromagnetic pole pitch' [16] of the rotary part.

When only the rotary part of the 2DoF-DDIM is energised, the distribution of the magnetic field at the outgoing end of the mover for rotary motion, where is the boundary between the rotary and linear parts, is shown in Fig. 10*a*. In addition, when both parts of the 2DoF-DDIM are energised, the distribution of the magnetic field in the same region is shown in Fig. 10*b*. In Fig. 10, 180° on the abscissa expresses the longitudinal end of the rotary part, where the mover goes out of the rotary stator in the circumferential direction.

Fig. 10*a* shows that the rotary part magnetic field is beyond the region of the rotary stator (from 180° to 220° on the abscissa), which results in an electromagnetic pole pitch larger than the mechanical pole pitch of the rotary part, due to the breaking of the rotary stator core. According to [16], the equivalent electromagnetic pole pitch is $(0.359/2p + 1)$ times the mechanical pole pitch. Hence, a higher rotary speed beyond the synchronous rotary speed (750 r/min) is produced, which can be verified in Fig. 9*b* and Table 3. According to Fig. 10*b*, the RCMF overlaps with the end of the linear part magnetic field so that it does not affect the rotary motion. The electromagnetic pole pitch is close to the mechanical pole pitch. Further, a comparison of Figs. 10*a* and *b* shows that the LCMF is linked with the rotary part magnetic field to change the end of the rotary part magnetic field. In short, the magnetic-coupling effect is the reason for the decrease in the rotary speed and increase in its fluctuation.

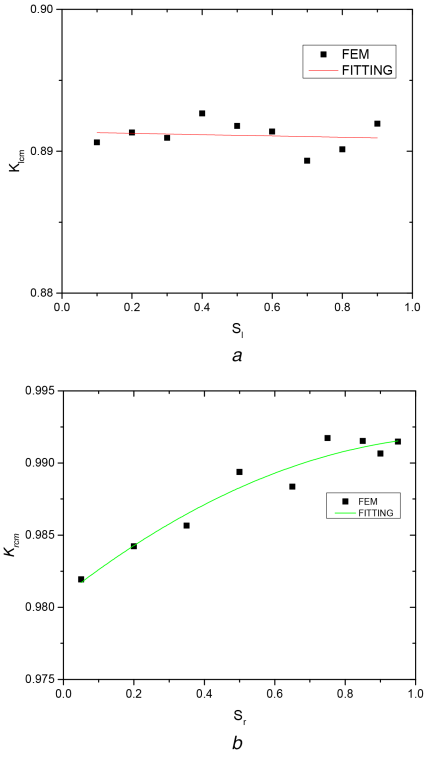

Fig. 11 *Speed coupling coefficient*
(a) Linear speed coupling coefficient, ***(b)*** Rotary speed coupling coefficient

In summary, the magnetic-coupling effect can cause lower speed and higher fluctuation of the 2DoF-DDIM according to the FEM results. Besides, the magnetic-coupling effect has a stronger effect on the rotary part than that on the linear part.

4.3 Speed coupling coefficient

For precise control of the 2DoF-DDIM, the magnetic-coupling effect on the motor speed should be researched. Hence, the speed coupling coefficients, K_{rcm} and K_{lcm}, are introduced to reflect the magnetic-coupling effect on motor speed. They can be determined as

$$\begin{cases} K_{\mathrm{lcm}} = \dfrac{V_{\mathrm{rcm}}}{V_{\mathrm{r}}} \\ K_{\mathrm{rcm}} = \dfrac{V_{\mathrm{lcm}}}{V_{\mathrm{l}}} \end{cases} \tag{3}$$

where V_{l} and V_{r} express the linear and rotary speeds without coupling, and V_{lcm} and V_{rcm} express the speeds with coupling, respectively.

The speeds of the 2DoF-DDIM under different operation conditions with and without coupling are simulated using the 3D finite-element model. Then, the speed coupling coefficients are calculated as shown in Fig. 11.

Fig. 11 shows that with an increase in rotary slip, K_{lcm} remains almost unchanged with the linear slip, while K_{rcm} increases nearly to 1. This result also verifies that the magnetic-coupling effect enhances with an increase in rotary speed, but has little relation with the linear speed. According to the curve fitting, K_{lcm} is close to a constant and K_{rcm} is a function related to rotary slip as

$$\begin{cases} K_{\mathrm{lcm}} = 0.89136 \\ K_{\mathrm{rcm}} = \mathrm{e}^{-0.0194 + 0.0194 S_{\mathrm{r}} - 0.0083 S_{\mathrm{r}}^2} \end{cases} \tag{4}$$

The ratio value between the mechanical pole pitch and the equivalent electromagnetic pole pitch is 0.9176, which is larger than the value of K_{lcm}. There are mainly two reasons for the phenomenon mentioned above: the decrease in the equivalent

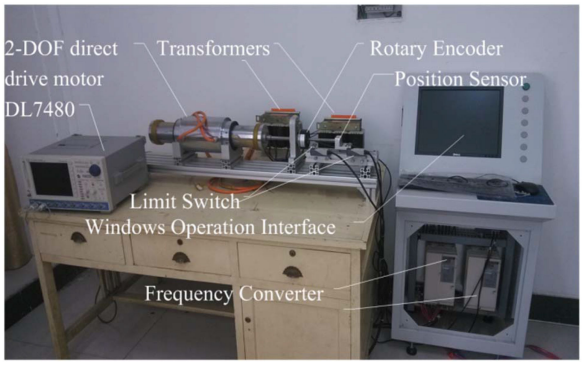

Fig. 12 *Test platform of 2DoF-DDIM*

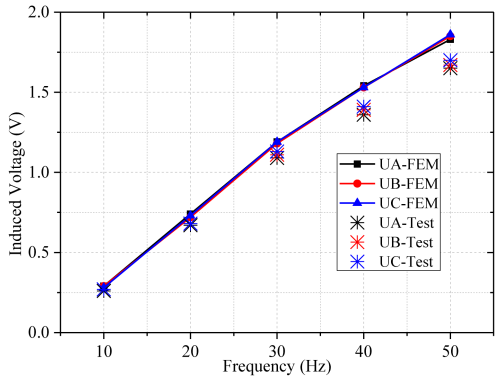

Fig. 13 *Induced voltages of linear part by test and FEM*

electromagnetic pole pitch of the rotary part caused by coupling, and the decrease effect on the rotary speed caused by the LCMF which is similar to the decrease in the linear speed caused by the RCMF. The curves of K_{rcm} and K_{lcm} also show that the stronger the coupling magnetic field is, the more obvious the magnetic-coupling effect will be. Further, we can conclude that the rotary part is more affected by the magnetic-coupling effect than the linear part from $K_{lcm} < K_{rcm}$. Besides, the introduction of the speed coupling coefficients is significant for the accuracy of the 2DoF-DDIM control system.

5 Experiment validation

A simple test platform of the 2DoF-DDIM is set up and experimental tests are carried out on the prototype of the motor, as shown in Fig. 12. The outputs of the frequency converter are controlled by the windows operation interface and transmitted to the prototype of the 2DoF-DDIM through the transformers.

There is no suitable 2DoF speed controller for the laboratory model of a 2DoF-DDIM. Therefore, it is technically difficult to measure the coupling effect of a 2DoF-DDIM at a constant rotary or linear speed. However, the zero linear speed can be achieved by the collision between the mover and the stator ends. Hence, the tests in which only the linear part is energised by AC sources with different frequency (from 10 to 50 Hz) are performed under zero linear speed. Then the induced voltages under different linear sources can be measured by the DL7480. A comparison of the FEM analysis and the test results is shown in Fig. 13.

Fig. 13 shows that the FEM analysis results coincide uniformly with the test results, which validates the finite-element model and magnetic-coupling effect of the 2DoF-DDIM.

6 Conclusion

This paper fully researches the special feature caused by the coupling magnetic field of the 2DoF-DDIM. The 3D finite-element model is established to determine the coupling magnetic field, induced voltages and currents, torque (or force) and speed developed by the motor under the conditions of with and without coupling. The magnetic-coupling effect enhances with the source frequency and the rotary speed, in which the former has been validated by tests. Besides, the magnetic-coupling effect leads to a decrease of torque (or force) and speed, and an increase of their fluctuations. Besides, the influence of the coupling magnetic fields on the motor performance, which agrees with the speed coupling coefficient, enhances with the coupling magnetic field intensity.

In the future, we will establish the control system of a 2DoF-DDIM. This research will be considered in the control algorithm to improve the control accuracy.

7 Acknowledgments

This work was supported by National Natural Science Foundation of China under grant nos. 51777060 and 51277054, Henan Natural Science Foundation of China under grant no. 162300410117.

8 References

[1] Sato, Y.: 'Development of a 2-degree-of-freedom rotational/linear switched reluctance motor', *IEEE Trans. Magn.*, 2007, **43**, (6), pp. 2564–2566

[2] Li, S.Y., Cheng, K.W.: 'A new two-degree of freedom switched reluctance motor for electric vessel'. Sixth Int. Conf. Power Electronics Systems and Applications (PESA), Hong Kong, 2015, pp. 1–6

[3] Amiri, E.: 'Circuit modeling of double-armature rotary- linear induction motor'. IECON 2014–40th Annual Conf. IEEE Industrial Electronics Society, 2014

[4] Amiri, E., Gottipati, P., Mendrela, E.A.: '3D space modeling of rotary-linear induction motor with twin-armature'. 2011 1st Int. Conf. Electrical Energy Systems (ICEES), 2011

[5] Amiri, E., Jagiela, M., Dobzhanski, O., *et al.*: 'Modeling dynamic end effects in rotary armature of rotary-linear induction motor'. 2013 IEEE Int. Electric Machines & Drives Conf. (IEMDC), 2013

[6] Dobzhanskyi, O., Amiri, E., Gouws, R.: 'Comparison analysis of electric motors with two degrees of mechanical freedom: PM synchronous motor vs induction motor'. Int. Young Scientists Forum on Applied Physics and Engineering, 2016

[7] Jin, P., Yuan, Y., Jian, G., *et al.*: 'Static characteristics of novel air-cored linear and rotary halbach permanent magnet actuator', *IEEE Trans. Magn.*, 2014, **50**, (2), pp. 977–980

[8] Jin, P., Lin, H., Fang, S., *et al.*: 'Decoupling control of linear and rotary permanent magnet actuator using two-directional d-q transformation', *IEEE Trans. Magn.*, 2012, **48**, (10), pp. 2585–2591

[9] Tanaka, S., Shimono, T., Fujimoto, Y.: 'Optimal design of length factor for cross-coupled 2-DOF motor with halbach magnet array'. 2015 IEEE Int. Conf. Mechatronics (ICM), 2015, pp. 529–534

[10] Pan, J.F., Cheung, N.C., Cao, G.: 'A rotary-linear switched reluctance motor'. 3rd Int. Conf. Power Electronics Systems and Applications, 2009

[11] Pan, J.F., Cheung, N.C., Cao, G.: 'Investigation of a rotary-linear switched reluctance motor'. XIX Int. Conf. Electrical Machines – ICEM 2010, Rome, 2010

[12] Pan, J.F., Zou, Y., Cheung, N.C.: 'Performance analysis and decoupling control of an integrated rotary–linear machine with coupled magnetic paths', *IEEE Trans. Magn.*, 2014, **50**, (2), pp. 761–764

[13] Si, J., Feng, H., Ai, L., *et al.*: 'Design and analysis of a 2-DOF split-stator induction motor', *IEEE Trans. Energy Convers.*, 2015, **30**, (3), pp. 1200–1208

[14] Si, J., Xie, L., Cao, W., *et al.*: 'Performance analysis of the 2DoF direct drive induction motor applying composite multilayer method', *IET Electr. Power Appl.*, 2017, **11**, (4), pp. 524–531

[15] Si, J., Xie, L., Xu, X., *et al.*: 'Static coupling effect of a two-degree-of-freedom direct drive induction motor', *IET Electr. Power Appl.*, 2017, **11**, (4), pp. 532–539

[16] Si, J., Al, L., Xie, L., *et al.*: 'Characteristic analysis of no-load speed of linear induction motor', *Electr. Mach. Control*, 2014, **18**, (7), pp. 37–43

9. Appendix

The derivation of (1) is as follows.

The rotary part of the 2DoF-DDIM is converted into a simplified model as shown in Fig. 14 with the following assumptions:

(1) The relative permeability, μ_r, of the arc armature core in the rotary part of 2DoF-DDIM is assumed to be infinitely great, so the conductivity, γ_r, is infinitely small.

(2) The impact of the linear stator slot is ignored while analysis the coupling magnetic field in the rotary part.

(3) The armature and mover curvature are ignored.

(4) The three-phase symmetrical sinusoidal current is connected to the armature winding, and all the electromagnetic volumes are characterised by sinusoidal variation.

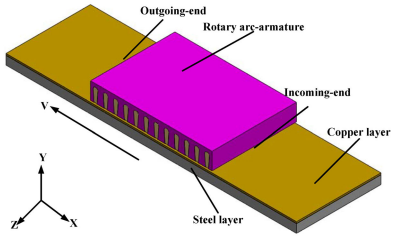

Fig. 14 *Simplified model of rotary part*

The equations of the vector magnetic potential are shown as

$$\begin{cases} \nabla^2\dot{A}_{mx} - \mathrm{j}\mu_0\gamma\omega_1\dot{A}_{mx} = -\mu_0\dot{J}_{mx} \\ \nabla^2\dot{A}_{my} - \mathrm{j}\mu_0\gamma\omega_1\dot{A}_{my} - \mu_0\gamma v\left(\dfrac{\partial A_{my}}{\partial x} - \dfrac{\partial A_{mx}}{\partial y}\right) = -\mu_0\dot{J}_{my} \\ \nabla^2\dot{A}_{mz} - \mathrm{j}\mu_0\gamma\omega_1\dot{A}_{mz} - \mu_0\gamma v\left(\dfrac{\partial A_{mz}}{\partial x} - \dfrac{\partial A_{mx}}{\partial z}\right) = -\mu_0\dot{J}_{mz} \end{cases} \tag{5}$$

where $\dot{A}_m = \dot{1}_x\dot{A}_{mx} + \dot{1}_y\dot{A}_{my} + \dot{1}_z\dot{A}_{mz}$ denotes the complex amplitude of the vector magnetic potential, μ_0 denotes the vacuum permeability, γ represents the relative electrical conductivity of the mover, w_1 stands for angular frequency, and v denotes rotary speed of the mover.

As indicated by the above coupling magnetic field model and assumed conditions, $\dot{A}_{mx} = \dot{A}_{mz} = 0$ and $\dot{A}_m = \dot{A}_{my}$. When the rotary part is the only powered of the system, the electrical current density in the coupling magnetic field is will be $\dot{J}_m = 0$. When they are substituted into the equation set of the vector magnetic potential (5), the vector magnetic potential in the coupling magnetic field region can be derived as

$$\frac{\mathrm{d}^2\dot{A}_m}{\mathrm{d}^2x^2} - \mathrm{j}\mu_0\lambda w\dot{A}_m - \mu_0\gamma v\frac{\mathrm{d}\dot{A}_m}{\mathrm{d}x} = 0 \tag{6}$$

The general solution of (4) is

$$\dot{A}_e = \dot{C}_1\mathrm{e}^{(\sqrt{\eta_2^2+\mathrm{j}G}+\eta_2)\alpha x} + \dot{C}_2\mathrm{e}^{-(\sqrt{\eta_2^2+\mathrm{j}G}-\eta_2)\alpha x} \tag{7}$$

where $\eta_2 = (\mu_0\gamma v)/\alpha$, $G = \mu_0\gamma_2 w_1\Delta/\delta\alpha^2$, γ_2 denote the conductivity of the mover, δ represents the equivalent electromagnetic air-gap, Δ denotes the thickness of the conductor plant of the mover, $\dot{C}_1$ and $\dot{C}_2$ stand for complex constants of the integrals to be confirmed.

According to $\dot{A}_{mo}\big|_{x=\infty} = 0$ in the region of the outgoing-end of the mover, it can be obtained that:

$$\begin{cases} \dot{C}_1 = 0 \\ \dot{A}_{mo} = \dot{C}_2\mathrm{e}^{-(\sqrt{\eta_2^2+\mathrm{j}G}-\eta_2)\alpha x} \end{cases} \tag{8}$$

where $0 \le x \le 2p\tau$.

According to $\dot{A}_{mi}\big|_{x=-\infty} = 0$ in the region of the incoming-end of the mover, it can be obtained that:

$$\begin{cases} \dot{C}_2 = 0 \\ \dot{A}_{mi} = \dot{C}_1\mathrm{e}^{-(\sqrt{\eta_2^2+\mathrm{j}G}+\eta_2)\alpha x} \end{cases} \tag{9}$$

where $-4p\tau \le x \le -2p\tau$.

Since the simplified model is obtained by an equivalent plate model of the 2DoF-DDIM, the vector magnetic potential in the coupling magnetic field is the superposition of the vector magnetic potential in the outgoing-end and the incoming-end. Thus, the complex amplitude of the vector magnetic potential in the coupling magnetic field can be expressed as

$$\begin{aligned} \dot{A}_m &= \dot{A}_{mi} + \dot{A}_{mo} \\ &= \dot{C}_1\mathrm{e}^{(\sqrt{\eta_2^2+\mathrm{j}G}+\eta_2)\alpha(x-4p\tau)} + \dot{C}_2\mathrm{e}^{(\sqrt{\eta_2^2+\mathrm{j}G}-\eta_2)\alpha x} \end{aligned} \tag{10}$$

where $0 \le x \le 2p\tau$.

Therefore, the magnetic flux density of the coupling magnetic field can be calculated according to $B_m = \partial\dot{A}_m/\partial x$, as shown in (9):

$$B_m = \dot{C}_1 m_1\mathrm{e}^{m_1(x-4p\tau)} - \dot{C}_2 m_2\mathrm{e}^{-m_2 x} \tag{11}$$

where

$$\begin{cases} m_1 = \sqrt{\mu_0^2\gamma^2v^2 + \mathrm{j}\dfrac{\mu_0 w\gamma_2\Delta}{\delta}} + \mu_0\gamma v \\ m_2 = \sqrt{\mu_0^2\gamma^2v^2 + \mathrm{j}\dfrac{\mu_0 w\gamma_2\Delta}{\delta}} - \mu_0\gamma v \end{cases}$$

Replace x to θ through coordinate conversion, the equation becomes:

$$B_m = \dot{C}_1 m_1\mathrm{e}^{m_1(\theta-2\pi)} - \dot{C}_2 m_2\mathrm{e}^{-m_2\theta} \tag{12}$$

where $0 \le \theta \le \pi$.